A Grouser Spacing Equation for Determining Appropriate Geometry of Planetary Rover Wheels

Krzysztof Skonieczny, Scott J. Moreland, and David S. Wettergreen

***Abstract*— Grousers, sometimes called lugs, are recognized as a way to improve wheel performance and traction, but there have been, to date, no comprehensive guidelines for choosing grouser patterns. This work presents a quantitative expression for determining appropriate grouser spacing for rigid wheels. Past empirical studies have shown that increasing grouser height and number can improve performance, to a point. The newly proposed grouser spacing equation is based on observations that wheels with an inadequate number of grousers induce forward soil flow ahead of the wheel, and thus rolling resistance. The equation relates geometric wheel parameters (wheel radius, grouser height and spacing) and operating parameters (slip and sinkage), and predicts a maximum allowable grouser spacing (or, equivalently, a minimum number of grousers). Experiments with various grouser heights and numbers demonstrate good correspondence to the proposed equation, as increases in number of grousers beyond the predicted minimum number stop improving performance. A grouser spacing equation is particularly useful for designing efficient wheels. The proposed relation includes slip and sinkage, parameters that cannot be assumed constant or known a priori, but this work shows that wheels designed using the proposed equation are robust to changing operating scenarios even if they degrade beyond estimated nominal conditions.**

I. Introduction

The entrapment and eventual loss of the Spirit Mars Exploration Rover (MER) in soft soil is a poignant reminder that mobility and vehicle-soil interaction is hardly a solved problem for planetary rovers. The loose granular regolith on Mars and the Moon can at times induce excessive slip, which is energy-sapping and unpredictably hazardous.

Due to mass and volume constraints imposed by space missions, Mars rovers have used wheels that are rigid and relatively small. Although wheels with large diameters and compliance exhibit higher performance in most conditions [1,2], this additional performance may not be worth the extra mass and volume in the context of planetary missions. To enhance performance of these small rigid wheels, the Mars rover wheels have utilized grousers, as seen in Fig. 1.

The use of features, such as grousers, on wheel rims has been relied upon for increasing traction of mobility platforms in a wide range of applications. Performance measurements for use in loose, granular soil have shown tractive gains for many implementations of these features [3].

Research supported by NASA.

K. Skonieczny, S. J. Moreland, and D. S. Wettergreen are all with the Carnegie Mellon University Robotics Institute, Pittsburgh, PA 15217 USA (for correspondence contact K. Skonieczny: kskoniec@cmu.edu).

Figure 1. Mars rover wheels with various grouser patterns. From left to right: MER, Sojourner, and Mars Science Laboratory (MSL). [NASA JPL]

There have been, to date, no comprehensive guidelines for choosing grouser patterns. This leads to a wide variety of grouser shapes, sizes, and styles implemented in practice (e.g. the three different wheels seen in Fig. 1), as well as an assortment of ongoing research on the subject.

Bauer et al [4] showed that increasing the number of grousers can increase drawbar pull (i.e. net traction: wheel thrust less resistance) for a rigid wheel in dry sandy soil. Liu et al [5] also demonstrated increasing drawbar pull as the number of grousers is increased, and showed that grouser height can also improve traction. Iizuka et al [6] presented further evidence suggesting that increasing grouser height increases drawbar pull. Recently, Sutoh et al [7] demonstrated that there is a limit to the gains attainable from increasing the number of grousers. They also showed that traction gains from grousers are greater than those provided by a wheel with simply a larger effective diameter, as some past literature had suggested would be the case.

Recent related work published by the authors [8] suggests that the increases in drawbar pull seen when the number of grousers is increased can be explained by a reduction in forward soil flow in front of the wheel, and thus decreased rolling resistance. The following section of this paper reviews this result, and subsequent sections build on it to develop a new expression capturing the relevant geometric relations governing the performance of wheels with grousers.

An expression that determines appropriate grouser geometry for increasing drawbar pull of planetary rovers is useful in at least two distinct ways: increased traction can mitigate risks of entrapment for planetary rovers, and reduced rolling resistance can increase overall power

efficiency and thus achieve higher scientific return in power-constrained planetary space missions.

II. Grousers for Reducing Rolling Resistance

A. Soil shear imaging experimental technique

The motion of loose granular soil influenced by wheels with grousers is investigated using a novel imaging technique.

The experimental apparatus consists of a glass-walled soil bin filled with GRC-1 lunar simulant, a wheel, an actuated horizontal axis of motion and a high-speed camera (Fig. 2). Wheel rotations are velocity-controlled in coordination with the horizontal axis to create a commanded, constant slip as the wheel travels forward. The forced horizontal axis motion is analogous to motion induced on a wheel by the rest of a rover. A linear rail allows the wheel to translate freely in the vertical direction allowing for natural sinkage to occur. This also allows for the transmission of a deadweight normal load to be applied to the wheel. Details of the wheel module are shown in Fig. 3.

A 6-d.o.f. force/torque sensor is incorporated to measure the reaction loads in all directions. Sinkage is also measured via an optical encoder affixed to the vertical free linear axis. All telemetry; wheel angular velocity, travel velocity, slip, sinkage, load and power are logged simultaneously at 20Hz or higher.

The test wheel is pressed against a sheet of tempered glass that extends to the depth of the soil bin. The test wheel is of half the width of the actual wheel of interest, and correspondingly half the payload weight is applied. This setup simulates a full wheel in unconstrained conditions, assuming a plane of symmetry at its centerline. Low shearing resistance between the implement and glass boundary is achieved by using tempered glass with a high hardness surface and by the low pressure of the soil particles against the glass wall.

A digital SLR camera with a 50mm macro lens is used to image the soil where it interfaces with the wheel, logging frames simultaneously with the rest of the telemetry. A frame rate of 8 frames-per-second is used and is sufficiently fast for the slow implement speeds. The camera is mounted perpendicular to the soil bin glass wall and travels with the implement in the horizontal direction as the carriage moves. External halogen flood lights at a high angle (from the normal) to the glass illuminate the soil particles.

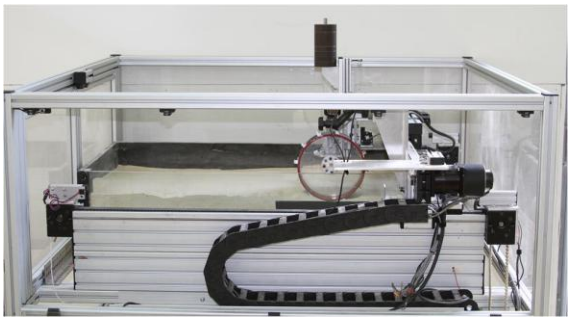

Figure 2. Glass-walled soil bin with horizontal axis of motion.

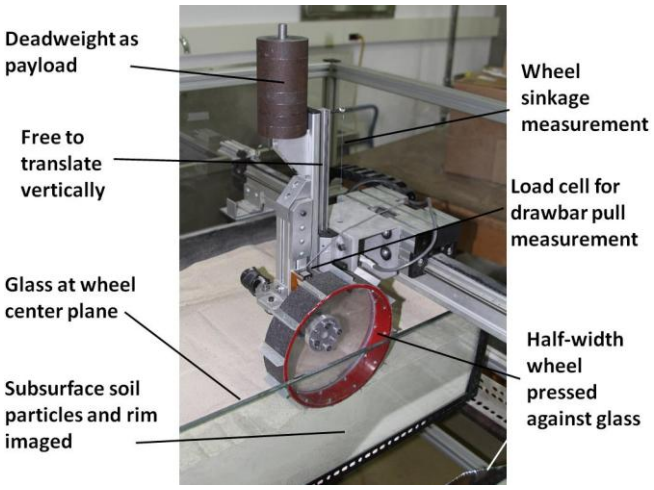

Figure 3. Detail of wheel module in soil bin.

Image processing comprises of optical flow and clustering. An optical flow algorithm [9] tracks displacement of soil regions relative to a prior frame and calculates a motion vector at each pixel. Initial clustering separates each image into "soil" and "not soil" regions. Additional processing and output is continued only for "soil" regions. The magnitude of flow at each pixel of the soil regions is calculated from the optical flow vector fields. Soil flow is clustered into "significant" and "insignificant" magnitudes of motion. No explicit threshold is used to demarcate these clusters, but rather automatically adaptive *k*-means clustering (a cluster analysis method often used in computer vision and data mining) is used. The shear interface is derived from the boundary between significant and insignificant motions. Soil flow direction is calculated from the optical flow vector fields, for soil regions exhibiting significant soil flow. Soil flow in any direction (360 degrees) is visualized, and an additional boundary is identified at points where the soil transitions between forward and rear flow. Fig. 4 shows sample output of the process, showing soil flow magnitude, shear interface between significant and insignificant flow, soil flow direction (within region of significant flow), and boundary between forward and rear flow.

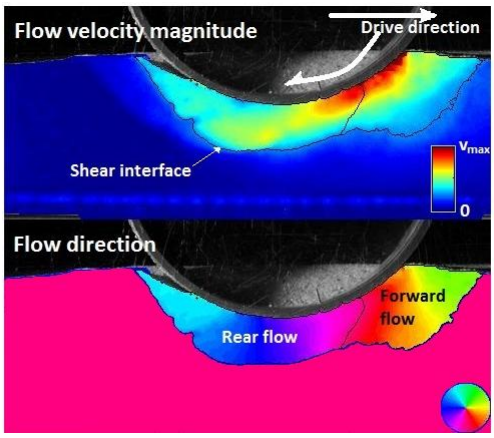

Figure 4. Sample processed output for driven wheel. Soil flow speed (upper) is denoted from blue (static) to red (max. speed). Soil flow direction (lower) within the shear interface is denoted according to the color wheel in the bottom right corner.

B. *Periodic forward flow*

Soil flow beneath wheels with various grouser size and spacing were observed using the aforementioned experimental technique. Soil response is strongly periodic, matching the frequency with which grousers encounter the terrain, as seen in Fig. 5.

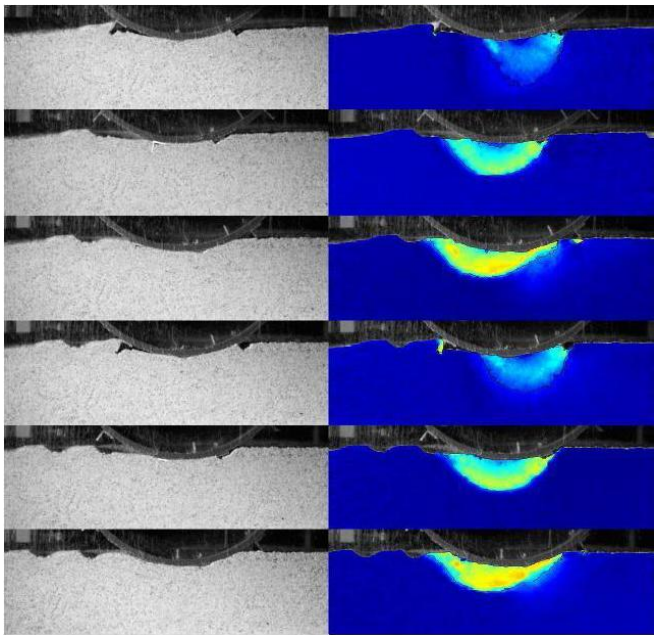

Figure 5. Soil shearing induced by grousers is strongly periodic. Time lapse photos and shear imaging output for two grouser cycles are shown.

Grouser spacing affects the way soil shears within each period of interaction. A greater range of soil motion is observed with larger grouser spacing (i.e. fewer grousers). As the number of grousers is increased and each individual interaction shortens, the periodicity of the soil response becomes less prevalent. This is observed specifically in terms of forward flow of the soil.

Fig. 6 shows two snapshots from a period of soil shearing with a wheel with 16 grousers. The soil flow direction plot from the snapshot on the left shows forward flow in front of the wheel. At a later moment, the snapshot on the right shows no forward flow. Analysis of the direction plots reveals this periodic appearance and disappearance of forward flow. Analysis of the drawbar pull data shows corresponding dips and rises in net traction.

A wheel with 48 grousers exhibits much smaller variations in drawbar pull across its period of grouser interaction, and images show no evidence of periodic forward flow. Fig. 7 shows a snapshot from experiments with such a wheel, with flow direction representative of soil flow observed throughout the interaction cycle.

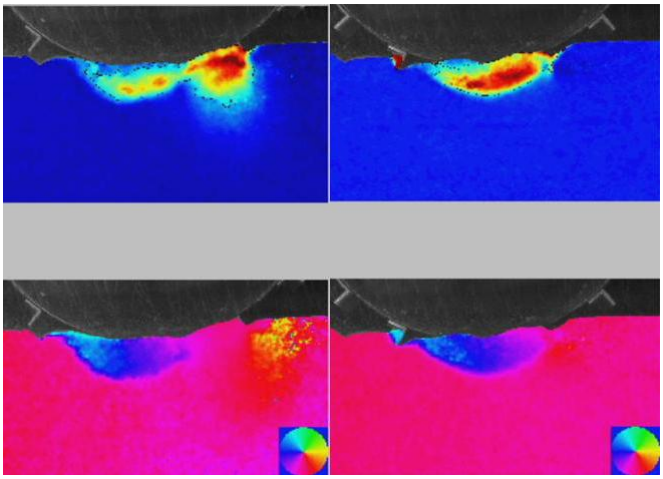

Figure 6. Periodic soil flow induced by a wheel with 16 grousers. Soil flow direction plots (lower plots) show forward flow periodically appearing and disappearing.

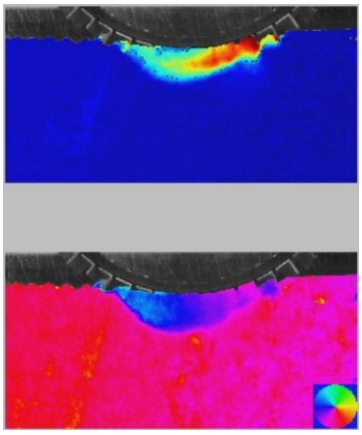

Figure 7. Snapshot of soil flow induced by a wheel with 48 grousers. No periodic forward flow observed.

As the periodic appearance of forward flow corresponds to temporary increases in resistance and thus drops in drawbar pull, an expression that predicts such increases in resistance and avoids them with appropriate grouser geometry would be beneficial for designing efficient wheels. The remainder of this paper discusses a novel formulation of just such an expression.

III. Grouser Spacing Equation

The intuition guiding the search for a grouser spacing equation is an endeavor to ensure grousers encounter soil ahead of a wheel before the wheel rim does. When a wheel rim encounters soil it bulldozes it forward and compacts it, producing resistance, in addition to shearing it to produce thrust. Grousers, on the other hand, have a net rearward motion near the bottom of a rotating wheel, and thus pull soil back and constrain it from undergoing resistive forward flow.

While deriving an expression for grouser geometry, parameters that include dimensions of length are normalized by wheel radius to keep equations dimensionless and slightly simpler. Normalized parameters are denoted with a hat (i.e.

$\hat{x} = x/r$). Table I summarizes relevant parameters, and Fig. 8 shows them in a diagram.

TABLE I. PARAMETERS FOR GROUSER GEOMETRY EXPRESSION.

Parameter	Symbol	Symbol for normalized parameter
Wheel radius	r	1
Grouser height	h	$\hat{h}$
Wheel sinkage	z	$\hat{z}$
Wheel linear velocity	v	$\hat{v}$
Wheel angular velocity	ω	n/a
Angular grouser spacing	ϕ	n/a
Wheel slip	i	n/a

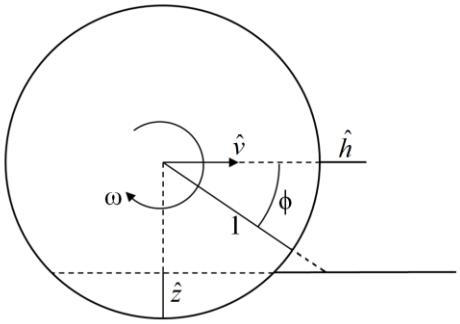

Figure 8. Wheel parameters with lengths normalized by wheel radius.

As a grouser pushes into soil, it clears a space in front of the wheel that the wheel rim does not encounter until it has translated horizontally. To ensure the next grouser encounters soil before the wheel rim does, the wheel must rotate by an angle of ϕ before it translates horizontally by a distance of $\overline{BC}$ (points *B* and *C* denoted in Fig. 9). This is expressed:

$$\frac{\phi}{\omega} < \frac{\overline{BC}}{\hat{v}} \quad \text{or} \quad \phi < \frac{\omega \overline{BC}}{\hat{v}} \tag{1}$$

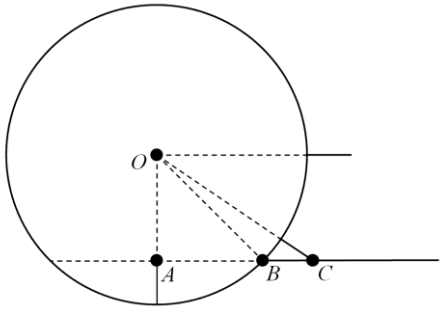

Figure 9. Normalized wheel with key geometric points called out.

Applying Pythagorean theorem to triangles *OAC* and *OAB*, $\overline{BC}$ can be expressed in terms of wheel parameters:

$$\overline{BC} = \overline{AC} - \overline{AB} = \sqrt{\left(1+\hat{h}\right)^2 - \left(1-\hat{z}\right)^2} - \sqrt{1-\left(1-\hat{z}\right)^2} \tag{2}$$

Slip is a useful parameter for capturing the relationship between rotational and translational velocities [2]:

$$i = 1 - \frac{v}{r\omega} = 1 - \frac{\hat{v}}{\omega} \quad \text{or} \quad \frac{\omega}{\hat{v}} = \frac{1}{1-i} \tag{3}$$

Substituting (2) and (3) into (1) yields:

$$\phi < \frac{1}{(1-i)}\left(\sqrt{\left(1+\hat{h}\right)^2 - \left(1-\hat{z}\right)^2} - \sqrt{1-\left(1-\hat{z}\right)^2}\right) \tag{4}$$

Equation (4) presents a grouser spacing equation that enables grousers to encounter soil before the wheel rim does. It relates wheel geometry parameters (grouser height and spacing, wheel radius) to operating parameters (slip and sinkage).

At this point it is prudent to ensure that the rim encounters the soil ahead of the wheel at point *C* first, as (1) implicitly assumes, not at another point deeper below the surface. This can be confirmed by geometric inspection. Consider first a case where the wheel is operating at 100% slip. The space that is cleared ahead of the wheel in this case takes the shape of an arc of radius equal to $r + h$. Imagining the wheel rim (radius r) subsequently translated horizontally (assuming constant sinkage), the rim encounters soil at point *C* because the curvature of the soil is less than that of the rim, and the wheel center is above the soil level (Fig. 10). When slip is less than 100%, as in the vast majority of cases, the soil curvature will be even closer to vertically down.

Soil might not, in some conditions, retain its shape perfectly, but the assumption that it does is an approximation that is required to keep the grouser spacing equation practical. The resulting grouser spacing should be treated as a useful estimate, not a precise calculation.

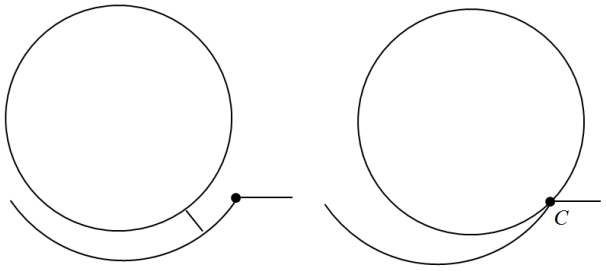

Figure 10. Grousers always cut soil at a curvature less than the wheel rim's curvature, so the rim always encounters the soil at point C.

IV. EXPERIMENTAL RESULTS

Experiments demonstrate the predictive power of the proposed grouser spacing equation. Experiments utilize a wheel with 114 mm radius and 57 mm width (pressed against glass wall of apparatus as described in Section II.A). This wheel size is relevant to planetary rovers in that it is just slightly smaller than MER wheels, which have 125 mm radius and 80 mm half-width, for comparison. Grousers of

different heights, 13 mm (1/2”), 10 mm (3/8”), and 6 mm (1/4”) are tested. The number of evenly spaced grousers is varied between experiments, to 3, 6, 12, 16, 24, 32, or 48 (not all grouser numbers are tested for each grouser height – 13 mm and 10 mm grousers were tested first at 3 through 24 and 48; for 6 mm grousers, testing less than 24 grousers was deemed unnecessary and impractical, but tests with 32 grousers were added to have at least 3 test conditions). Resulting drawbar pull is measured.

Slip is prescribed to 20% for all tests, by controlling horizontal carriage speed and wheel angular speed. 20% slip is high enough to produce considerable thrust, without being so high as to induce undesirable levels of slip-sinkage. Sinkage is allowed to occur freely in the experiements, and is measured for each test condition. Tests with 13 mm grousers result in normalized sinkage, $\hat{z}$, of 0.10 (i.e. 10% of wheel radius) and those with 10 mm and 6 mm grousers have normalized sinkage of 0.08.

Knowing slip as well as normalized grouser height and sinkage for each set of tests enables prediction of appropriate grouser spacing using (4). Table II shows predicted maximum grouser spacing, and corresponding minimum number of grousers, for sets of experiments with different grouser heights.

TABLE II. PREDICTED MINIMUM NUMBER OF GROUSERS

Grouser height	$\hat{h}$	$\hat{z}$	i	Max. grouser spacing, ϕ, predicted	Corresponding min. number of grousers
13 mm	0.11	0.10	0.2	0.27 rad	24
10 mm	0.08	0.08	0.2	0.22 rad	29
6 mm	0.06	0.08	0.2	0.15 rad	42

Fig. 11 presents drawbar pull results for sets of experiments with different grouser heights. Each data point plotted in the figure is an average of 3 drawbar pull tests conducted at the given test condition.

The 13 mm and 10 mm grousers exhibit a similar trend with increasing number of grousers. As the number of grousers increases from 3 to 24, in both cases, drawbar pull rises. Comparing drawbar pull between tests with 24 and 48 grousers, though, shows no further improvement. This is consistent with the predicted minimum number of grousers of 24 and 29 (for 13 mm and 10 mm grousers, respectively). Once the minimum number of approximately 24 grousers is reached, additional grousers no longer provide further reductions in rolling resistance.

For 6 mm grousers, experiments show drawbar pull continuing to increase as the number of grousers is increased from 24 to 48. This again is consistent with the prediction listed in Table II, which puts the minimum number of these smaller grousers at approximately 42.

The proposed grouser spacing equation is thus consistent with experimental results, and appears that it may be a good prediction of the appropriate number of grousers required to reduce rolling resistance. Future experiments could confirm this result with greater confidence.

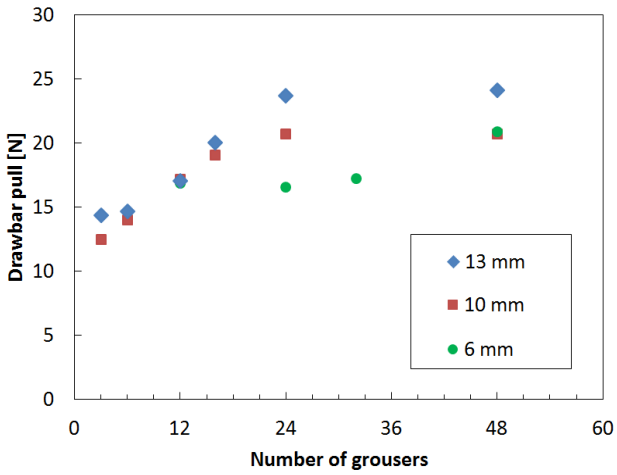

Figure 11. Drawbar pull vs. number of grousers for different grouser heights. For 13 mm and 10 mm grousers, drawbar pull first increases with number of grousers, but levels out with approximately 24 grousers. For 6 mm grousers, drawbar pull continues to increase between 24 and 48 grousers.

The reduction of rolling resistance may not be the only advantage of using grousers on a small rigid wheel. The difference in maximum drawbar pull for 13 mm and 10 mm grouser experiments suggests that grouser height may also impact thrust (which is the other half of drawbar pull). However, the differences in drawbar pull observed with varying number of grousers suggest that estimating the right number of grousers is very useful.

V. APPLICATION: WHEEL DESIGN

A practical application for a grouser spacing equation is the design of highly efficient rigid wheels, which are particularly useful for planetary rovers. It is clear how an expression relating geometric wheel parameters (wheel radius, grouser height and spacing) could be used for design. What may not be as immediately clear is how to handle operational parameters such as slip and sinkage.

Slip and sinkage are unlikely to be constant or even known for all likely operating scenarios ahead of time. This suggests that perhaps the usefulness of the proposed grouser spacing equation is limited to an academic exercise, but fortunately this is not the case. Estimating nominal slip and sinkage values can in fact still lead to robust design choices.

The minimum required number of grousers predicted by (4) decreases with increasing slip, so if slip were to increase beyond its nominal design point the current number of grousers would continue to satisfy the grouser spacing equation.

The minimum required number of grousers does increase with increasing sinkage, but (4) can nonetheless be shown to be dominated by slip. Sinkage is, in practice, related to slip and would not increase without slip increasing substantially.

A conservative estimate of a slip-sinkage relationship based on literature review [4, 10] is:

$$\hat{z} \le \frac{1}{2} i \tag{5}$$

Increasing slip from its nominal 20%, and correspondingly increasing sinkage according to (5), leads to overall operating conditions that continue to satisfy a nominally designed grouser spacing, as shown in Fig. 12.

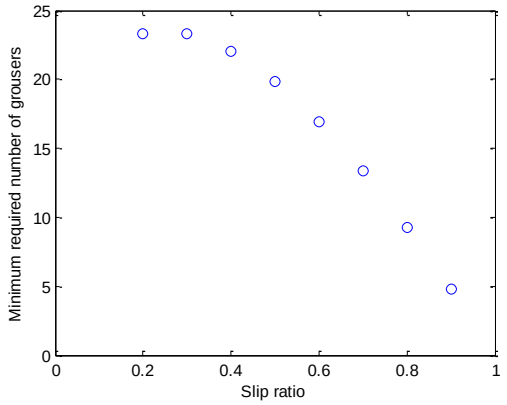

Figure 12. The minimum number of grousers required does not increase with increasing slip (even as sinkage is increased correspondingly). An appropriately designed wheel would thus be robust to deteriorating conditions.

Slip and sinkage from nominal operating conditions (either measured or estimated) can be used to design grouser spacing for a wheel, and if worse than nominal conditions are encountered, then at least the wheel will not start failing the grouser spacing equation and will not thus degrade performance even further.

For operations with a planetary rover on Mars, NASA JPL has collected a wealth of data from which nominal slip and sinkage could be estimated. Stereo pairs that include rover tracks, such as the example shown in Fig. 13, could be used to reconstruct the 3D track depth and ridges (created by the grousers) seen in the images.

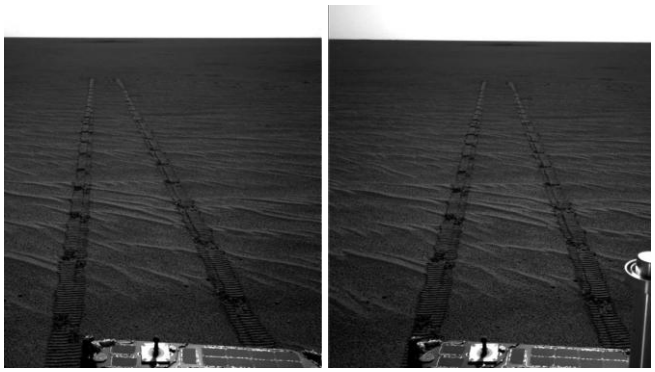

Figure 13. Left and right stereo pairs from MER Opportunity looking back at its tracks. Data like these could be used to calculate nominal slip and sinkage for Mars [NASA JPL].

VI. Conclusion

A grouser spacing equation is presented that relates geometric wheel parameters as well as operating parameters, and can be used to design efficient wheels:

$$\phi < \frac{1}{(1-i)}\left(\sqrt{(1+\hat{h})^2 - (1-\hat{z})^2} - \sqrt{1-(1-\hat{z})^2} \right)$$

This relation is especially applicable to planetary rovers, which tend to have relatively small rigid wheels (that are susceptible to causing resistive forward soil flow). It remains to be seen whether the relation is also useful for wheels that are less likely to cause forward flow, such as large-diameter or compliant wheels.

Future experimental work could investigate forward soil flow ahead of larger diameter wheels, and determine whether grousers provide similar advantages for such wheels.

As the grouser spacing equation requires an estimate of nominal operating parameters, namely slip and sinkage, it is recommended that future work look specifically at refining estimates of these parameters for Mars rovers based on existing MER data.

Acknowledgment

This work has been funded in part by NASA grant NNX07AE30G.

References

[1] M. G. Bekker, *Introduction to Terrain-Vehicle Systems*. Ann Arbor, MI: University of Michigan Press, 1969.

[2] J. Y. Wong, *Theory of Ground Vehicles*, 3rd edition. New York, NY:Wiley, 2001.

[3] L. Ding, Z. Deng, H. Gao, K. Nagatani, and K. Yoshida, "Planetary rovers' wheel-soil interaction mechanics: new challenges and applications for wheeled mobile robots," *J Intel. Serv. Robotics*, vol. 4, pp. 17-38, Jan. 2011.

[4] R. Bauer, W. Leung, and T. Barfoot, "Experimental and Simulation Results of Wheel-Soil Interaction for Planetary Rovers," *IEEE Int. Conf. Intel. Robots & Systems*, Edmonton, 2005, pp. 586-591.

[5] J. Liu, H. Gao, and Z. Deng, "Effect of straight grousers parameters on motion performance of small rigid wheel on loose sand," *Info. Tech. J.*, vol. 7, pp. 1125-1132, 2008.

[6] K. Iizuka, T. Yoshida, and T. Kubota, "Effect of tractive given by grousers mounted on wheels for lunar rovers on loose soil," *37th Ann. Conf. IEEE Industrial Elec. Soc.*, Melbourne, 2011, pp. 110-115.

[7] M. Sutoh, J. Yusa, T. Ito, K. Nagatani, and K. Yoshida, "Traveling performance evaluation of planetary rovers on loose soil," *J. Field Robotics*, doi: 10.1002/rob.21405, Jan. 2012.

[8] S. Moreland, K. Skonieczny, H. Inotsume, and D. Wettergreen, "Soil behavior of wheels with grousers for planetary rovers," *IEEE Aerospace*, Big Sky, 2012.

[9] M. J. Black, and P. Anandan, "The robust estimation of multiple motions: Parametric and piecewise-smooth flow fields," *CVIU*, vol 63, pp. 75-104, 1996.

[10] M. Lyasko, "Slip sinkage effect in soil-vehicle mechanics," *J. Terramechanics*, vol. 47, pp. 21-31, Feb. 2010.